Gas-assisted focused-ion-beam lithography of a diamond (100) surface

A. Datta, Yuh-Renn Wu,[a] and Y. L. Wang[b]
Institute of Atomic and Molecular Sciences, Academia Sinica, and Department of Physics, National Taiwan University, Taipei 106, Taiwan

(Received 20 January 1999; accepted for publication 25 August 1999)

A focused Ga-ion beam is used to conduct lithography on a diamond (100) surface with the assistance of various gases (Cl_2, O_2, and XeF_2). The beam-induced dilation and sputtering of the surface are measured by atomic force microscope. The dilation is found to be insensitive to the presence of assisting gases at low doses, while the sputtering is enhanced by O_2 and XeF_2 at high doses. The topographic evolution as a function of the ion dose is well described by a proposed semiempirical equation. Combining physical sputtering and XeF_2-assisted etching, the lithographic process has been used to fabricate submicron structures on diamond surfaces. © *1999 American Institute of Physics.* [S0003-6951(99)02943-5]

Among many unique properties of diamond, maximum hardness and low chemical reactivity lead to very special applications such as indenters and machining tools. Miniaturization of these objects is desirable but technologically challenging. With its large momentum, small beam diameter and high current density, the focused ion beam (FIB) appears to be a promising lithographic tool for creating such microscopic objects, especially when conducted in the presence of a gas for enhancing the etching.[1,2]

We have conducted FIB lithography on a diamond surface and studied the effects of Cl_2, O_2, and XeF_2 on the lithographic processes. We tried to identify an assisting gas[3] that significantly enhances the etching rate without compromising much of the spatial resolution of the FIB lithography. High-resolution lithography requires a delicate balance of the charging on the insulating diamond surface as well as careful control of the FIB instability, often caused by corrosive gas injection. In this letter, we report on the FIB-induced topographical evolution of the diamond surface, the enhancing effects of various assisting gases, and the fabrication of submicron-scale indenters.

A FIB system (Micrion 2500) with a 50 keV, 100 pA Ga ion beam under normal incidence is used to conduct the lithography[4] at room temperature (~300 K). An electron beam of ~80 eV is introduced to reduce the charging of the diamond surface. The gases are delivered through a nozzle with ~0.5 mm diam, positioned ~250 μm above the target area. The pressure for the assisting gas, as measured by a cold-cathode gauge ~50 cm away from the sample, is set at $\sim 1\times10^{-5}$ Torr (base pressure $\sim 5\times10^{-8}$ Torr). Beyond this pressure the FIB often becomes unstable. The FIB is digitally scanned across the target with a small dwell time of $T_{dt}=0.5$ μs, in order to minimize depletion of the adsorbed enhancing gas. The total time lapse (T_t) for the beam to be positioned at a particular pixel between two consecutive scans is determined by the total number of pixels to be addressed and the refresh time (T_{rf}) between two consecutive scans. Increasing T_{rf} will replenish more assisting gas that is removed by the previous FIB scan. The number of pixels are determined by the pixel spacing and, therefore, by the beam diameter, because significant overlap between two consecutive pixels is necessary for a semicontinuous etching. For a 100 pA beam, its diameter is ~70 nm, and a good choice for pixel spacing is ~50 nm. Therefore, the total number of pixels in a typical 3×3 μm^2 is 3600. For a choice of $T_{rf}=3$ ms, T_t is ~5 ms. The total gas exposure during the refreshing time is estimated to be ~0.3 L, assuming the local pressure of the assisting gas is $\sim 5\times10^{-5}$ Torr.

Natural diamond (100) samples are cleaned chemically,[5] blown dry in nitrogen flow, and mounted in the FIB chamber. The topographies of the ion-bombarded areas are measured in air by an (DI Nanoscope E) atomic force microscope (AFM) with typical lateral and height resolution of ~1 and ~0.1 nm, respectively. Figures 1(a) and 1(b) show representative AFM images of a mount created by ion-beam-induced dilation and a crater by XeF_2-assisted etching, respectively. The edge definition indicates that the spatial resolution of the FIB lithography is close to the beam diameter, implying adequate compensation of charging by flooding electrons leading to sub-100 nm lithography on the diamond surface.

Figure 2 shows the height *(h)* of the areas bombarded by different ion doses *(D)* in the presence of various assisting gases as well as physical sputtering. In all the cases, a protrusion[4,6,7] becomes observable in the bombarded area at $D=5\times10^{14}$ ions/cm^2, and it reaches a plateau ~20 nm at $D\sim1\times10^{17}$ ions/cm^2. For $D>2\times10^{17}$ ions/cm^2, a crater is created in the bombarded area. In this high-dose regime, the results for O_2 and XeF_2 start to deviate from that for the physical sputtering, with an enhancement factor of ~2 and ~4 in the etching rate, respectively, while that for Cl_2 remains identical.

The height h of the bombarded area is changed because of the ion-induced damage of the underlying lattice and sputtering of the surface. Including the effect of sputtering that moves the position of the surface forward and assuming that the dependence of r (depth in which the defect density maximizes) and σ (spread of the profile) on the ion dose can be

[a]Present address: Graduate Institute of Communication Engineering, National Taiwan University, Taipei 106, Taiwan.
[b]Electronic mail: ylwang@po.iams.sinica.edu.tw

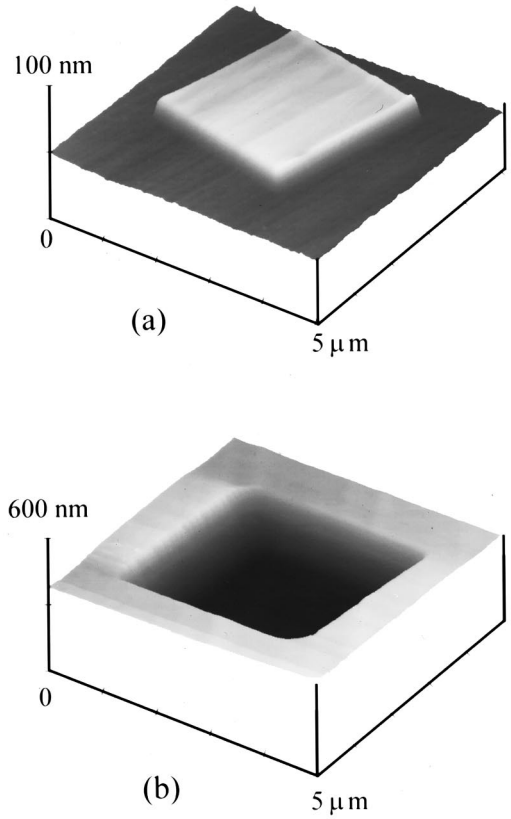

FIG. 1. AFM image of (a) a mount created by FIB bombardment (dose 1×10^{17} ions/cm^2) and (b) a crater created by XeF_2-assisted FIB etching (dose 1×10^{18} ions/cm^2).

neglected, the defect density distribution along the z axis can be approximated by

$$D_d(z)=\frac{Y_d}{\sqrt{\pi}}\int_0^D \exp\left\{-\frac{[z-r-S(D')D'/n(D')]^2}{2\sigma^2}\right\}dD', \tag{1}$$

where Y_d is the defect yield (i.e., the average number of defects produced per incident ion), $S(D')$ is the sputtering yield; and $n(D')$ is the density of the surface layer after the accumulative bombardment of some ion dose D'. To estimate the effect of the defects on h, we can assume that a dilated layer with its atomic density reduced by a factor of ϵ (dilation coefficient) is created under the surface when $D_d(z)$ is beyond a certain threshold D_0 for saturated dilation. If $S(D')/n(D')$ is known, the thickness of the dilated layer can be found by solving Eq. (1). Generally, S depends on n which changes with D'. However, for the condition of our physical sputtering experiment, S/n remains almost constant because S is approximately inversely proportional to n. Therefore, Eq. (1) can be approximated by

$$D_d(z)=\frac{Y_d}{\sqrt{\pi}}\left(\frac{n}{S}\right)\int_{(1/\sqrt{2}\sigma)(z-r)}^{(1/\sqrt{2}\sigma)[(S/n)D-z+r]}\exp(-x^2)dx. \tag{2}$$

For given D_0 and D, the increase in the thickness of the dilated layer (Δz_d) can be derived from Eq. (2). In the case of low ion dose ($SD/n \ll z-r$), it has an analytical solution: $\Delta z_d=2\sqrt{2}\sigma\epsilon[\ln(Y_dD/\sqrt{2\pi}\sigma D_0)]^{1/2}$. Generally, Eq. (2) can only be solved numerically. The combined effects of dilation and sputtering on the height can be expressed as

$$h(D)=\Delta Z_d(D)=\frac{S(D)}{n(D)}D. \tag{3}$$

Equations (2) and (3) suggest that *h(D)* can be approximated by a universal function provided the length scale *(h, z,* and *r)* and the dose *(D)* are measured in the unit of $\sqrt{2}\sigma$ and $\sqrt{2}\sigma n/S$, respectively. Since Δz_d becomes negligible for large D, S/n can be measured readily from high-dose experiments and used with σ from simulation[8] for rescaling of the ion dose. Figure 3(a) shows the experimental results in the normalized unit, where $\sqrt{2}\sigma=4.6$ nm. All the experimental data, including the results of gas-assisted etching, appear to fall on a single curve, suggesting the validity of a universal function for *h(D)*. The solid line in Fig. 3(a) is the best fit of Eq. (3) to the data for physical sputtering and Cl_2-assisted cases with $\epsilon=1.3$ and $Y_d/\sqrt{2\pi}\sigma D_0=1\times10^{-15}$ cm^2. The large ϵ indicates a very significant expansion of the dilated layer. Taking $Y_d\sim200$ from the simulation,[8] D_0 is $\sim1\times10^{23}$ cm^{-3}, which is close to the density of diamond. To be noted is that $S/n=9.1\times10^{22}$ (cm^3) as measured from physical sputtering in the high doses is essentially the same as that from the simulation.

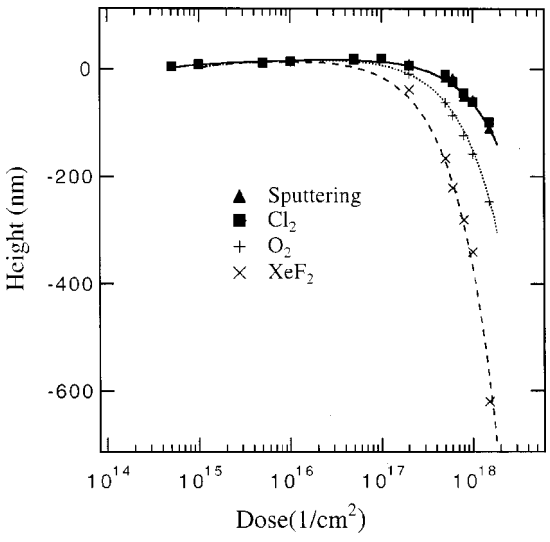

FIG. 2. Height of the bombarded area vs ion dose for various assisting gases and physical sputtering.

The processes involved in a gas-assisted etching are usually quite complex.[9] Molecular chlorine[10] has very little sticking probability to the diamond (100) surface, which could explain why for Cl_2 and physical sputtering the result is essentially the same. For O_2 and XeF_2, the molecules dissociatively chemisorb on the diamond (100) surface to create atomic oxygen and fluorine.[10–13] The effects can be quantified by calculating the sputtering yields from the depths of the craters created at high ion doses ($>5\times10^{17}$ ions/cm^2). For doses below 1×10^{17} ions/cm^2, h vs D are essentially the same for all the conditions used in our experiments, indicating that the dilation and the sputtering are not affected by the presence of these gases. To understand the implications of this interesting observation, we compare the results for gas-assisted etching with the predictions of Eq. (3) that describe *h(D)* for physical sputtering quite well. Using the normalized dose scale derived from high-dose experiments $\sqrt{2}\sigma n/S$ $(O_2)=2.5\times10^{16}$ and $\sqrt{2}\sigma n/S(XeF_2)=1.1\times10^{16}$

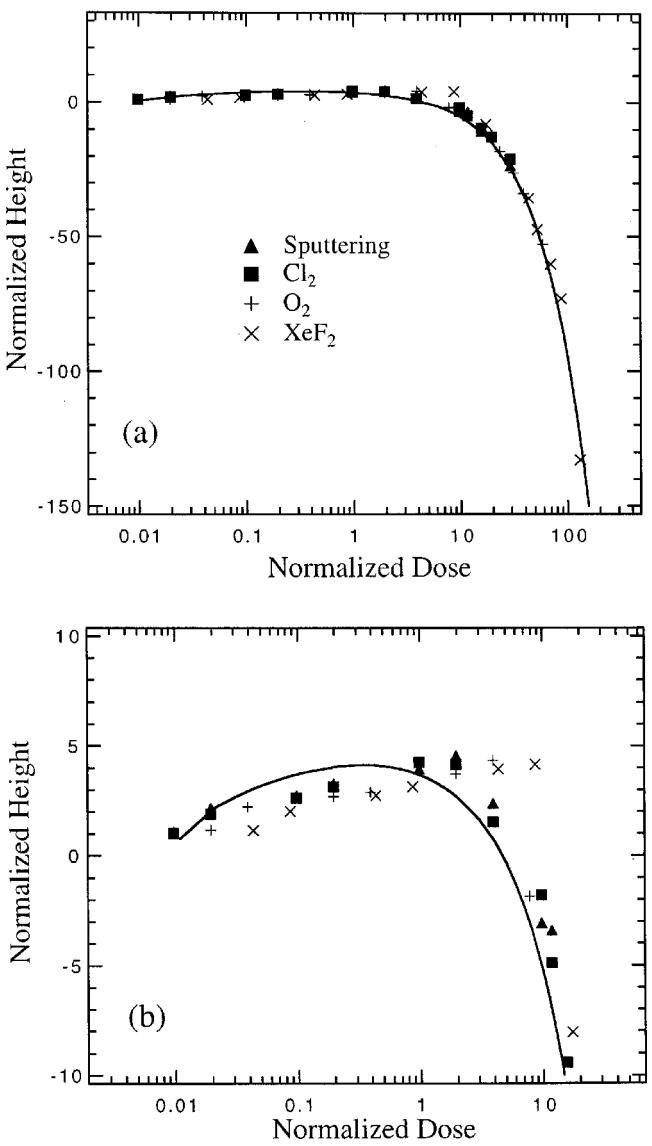

FIG. 3. (a) Normalized height vs normalized dose for various assisting gases and physical sputtering. Solid curve is the fitting of Eq. (3) to the results of physical sputtering and Cl_2-assisted etching. (b) Details of (a) showing the deviation in the medium-dose range for gases O_2 and XeF_2 from the universal behavior.

cm^{-2}, the results for these gas-assisted etchings are shown in Fig. 3. On a large scale [Fig. 3(a)], Eq. (3) appears to fit both physical sputtering and these results quite well. However, on a fine scale [Fig. 3(b)], clear deviations are observed in the medium normalized dose range (0.01–10). The deviation could be understood if *S/n* is no longer dose independent in the presence of the assisting gas.

The XeF_2-enhanced etching rate can be exploited for applications. We have employed XeF_2 etching in conjunction with physical sputtering for the fabrication of submicron indenters. Figure 4 shows an example of such an indenter. The side of the indenter is first defined by the FIB at higher resolution (~30 nm) using physical sputtering, and then

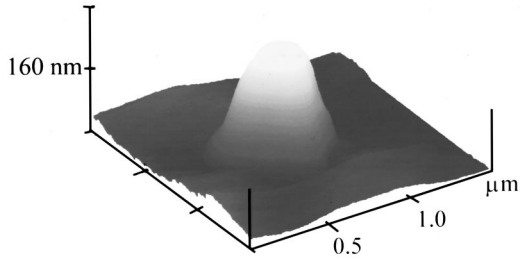

FIG. 4. AFM image of a submicron diamond indenter fabricated by FIB lithography.

XeF_2 is introduced to remove material further away from the tip. The resolution of the XeF_2-assisted etching is reduced to ~70 nm in order to achieve the desired enhancing effect and increased speed. Without the assistance of XeF_2, the relatively high dose needed for producing such an indenter usually leads to severe damage of its surface due to the tail of FIB profile.

In conclusion, we have studied FIB-induced dilation and sputtering of the diamond (100) surface with and without the presence of various gases. XeF_2-assisted etching, under suitable operating conditions, leads to an enhancement factor of 4, which can be utilized to create submicron structures with reduced ion damage. Beam-induced dilation is observed in the low-dose regime ($\leqslant 1\times 10^{17}$ ions/cm^2), while gas-assisted enhancement is observable only at the higher-dose regime. The gas-induced enhancement takes place when the near-surface region contains a high concentration of vacancies. Submicron diamond indenters are fabricated using a combination of physical sputtering and XeF_2-assisted etching.

The authors acknowledge the technical assistance received from the Micrion Corporation. This work has been partly funded by the National Science Council, Taiwan, R.O.C. (NSC 88-2112-M-001-024).

[1] Y. L. Wang and Z. Shao, in *Advances in Electronics and Electron Physics*, edited by P. W. Hawkes (Academic, Boston, 1991), Vol. 81, p. 177, and references therein.
[2] J. B. Wang and Y. L. Wang, Appl. Phys. Lett. **69**, 2764 (1996), and references therein.
[3] S. Kiyohara, I. Miyamoto, K. Kitazawa, and S. Honda, Nucl. Instrum. Methods Phys. Res. B **121**, 510 (1997).
[4] J. B. Wang, A. Datta, and Y. L. Wang, Appl. Surf. Sci. **135**, 129 (1998).
[5] R. E. Thomas, R. A. Rudder, and R. J. Markunas, J. Vac. Sci. Technol. A **10**, 2451 (1992).
[6] D. J. Oostra, R. P. van Ingen, A. Haring, A. E. de Vries, and G. N. A. van Veen, Appl. Phys. Lett. **50**, 1506 (1987).
[7] P. Schmuki, L. E. Erickson, G. Champion, B. F. Mason, J. Fraser, and C. Moessner, Appl. Phys. Lett. **70**, 1305 (1997).
[8] J. F. Zeigler and J. P. Biersack, SRIM (TRIM-90) Simulation package (1995), IBM Research, 28-024 Yorktown, NY, 10598.
[9] H. F. Winter and J. W. Coburn, Surf. Sci. Rep. **14**, 161 (1992), and references therein.
[10] A. Freedman, J. Appl. Phys. **75**, 3112 (1994).
[11] T. Yamada, T. J. Chuang, H. Seki, and Y. Mitsuda, Mol. Phys. **76**, 887 (1991).
[12] J. F. Morar, F. J. Himpsel, G. Hollinger, J. L. Jordan, and F. R. Mcfeely, Phys. Rev. B **33**, 1340 (1986).
[13] J. C. Lin (private communication).